Monthly climatology of the continental shelf waters of the South Atlantic Bight

Brian O. Blanton, Alfredo Aretxabaleta, Francisco E. Werner, and Harvey E. Seim
Department of Marine Sciences, University of North Carolina at Chapel Hill, Chapel Hill, North Carolina, USA

Received 21 August 2002; revised 8 April 2003; accepted 30 April 2003; published 15 August 2003.

[1] Monthly circulation of the South Atlantic Bight is diagnosed using a 3-D, shallow water, finite element model forced with monthly wind stress and hydrographic climatology. Temperature and salinity observations from the period 1950–1999 are objectively interpolated onto the model domain, and Comprehensive Ocean-Atmosphere Data Set (COADS) wind velocities from 1975–1999 are used to prescribe the model surface wind stress. The resulting monthly temperature and salinity fields compare favorably to existing shelf climatology. River discharge maxima are evident in the spring temperature and salinity fields, and the rapid heating and cooling of the shelf are captured. The diagnostic circulation is largely wind-driven in the inner and mid-shelf, and the Gulf Stream is apparent in the solutions on the outer shelf. We present the monthly fields, including the temporal and spatial distribution of available hydrographic data, the regional COADS data that provide surface wind stress forcing, the objective analysis, and the model response to these forcings. The hydrographic and velocity fields provide best-prior-estimates of the circulation for data assimilation studies in the region, as well as initial conditions for process-oriented prognostic model studies in the Georgia coastal region. *INDEX TERMS:* 4219 Oceanography: General: Continental shelf processes; 4255 Oceanography: General: Numerical modeling; 4512 Oceanography: Physical: Currents; *KEYWORDS:* climatology, objective analysis, South Atlantic Bight, finite element model

Citation: Blanton, B. O., A. Aretxabaleta, F. E. Werner, and H. E. Seim, Monthly climatology of the continental shelf waters of the South Atlantic Bight, *J. Geophys. Res.*, *108*(C8), 3264, doi:10.1029/2002JC001609, 2003.

1. Introduction

[2] The South Atlantic Bight (SAB) (Figure 1) region of the eastern United States coast extends from Cape Hatteras, North Carolina, to about Cape Canaveral, Florida. The continental shelf (shoreward of the 200-m isobath) is narrow on the northern and southern extremes (10–30 km) and broadens to about 120 km off the middle Georgia coast. The depth contours are largely parallel to the coast. The coast is permeated with rivers and tidal inlets, particularly from middle South Carolina to northern Florida. The coastal waters (shoreward of the 100-m isobath) are significantly influenced by atmospheric fluxes, buoyancy fluxes from rivers, tides, and the Gulf Stream. The Gulf Stream lies generally seaward of the 100-m isobath, but can influence the outer to mid-shelf (45- to 100-m isobath) region on weekly timescales [*Lee et al.*, 1981; *Lee and Atkinson*, 1983]. During spring, river discharge into the coastal waters is significant, generating less dense near-shore frontal zones with equatorward flows [*Blanton*, 1981]. While these general topographic and coastal features are not unique to the SAB, the presence of the Gulf Stream imposes a complicating influence on the SAB hydrographic and circulation characteristics.

0148-0227/03/2002JC001609

[3] The seasonal temperature and salinity (TS) and wind field characteristics in the SAB have been well characterized in previous studies. *Atkinson et al.* [1983] derived monthly fields of surface temperature and salinity and bottom temperature based on hydrographic observations accumulated over 1946–1980. (This study is our primary point of comparison.) Their results indicate that cross-shelf hydrographic properties can be broken into inner, mid-, and outer shelf regions depending on the mechanisms determining the property distributions. The Gulf Stream dominates the outer shelf; the mid-shelf is dominated by influences from the tides, wind field, and density forcing with frequent contributions from the Gulf Stream; the inner shelf is dominated by atmospheric fluxes, river discharge, and tidal mixing.

[4] The primary wind field climatology is that derived by *Weber and Blanton* [1980], and enhanced by *Blanton et al.* [1985], who split ship-of-opportunity records of wind speed and direction in the SAB into months and classified the results into seasons based on similarity of resulting surface wind stress patterns. They developed five seasonal wind field periods. Winter (November–February) mean winds are southeastward in the northern SAB and southward over the southern SAB. Spring (March–May) is a transition period for the hemispheric surface atmospheric pressure distribution with winds rotating toward the north in the central and northern SAB, while the winds in the southern

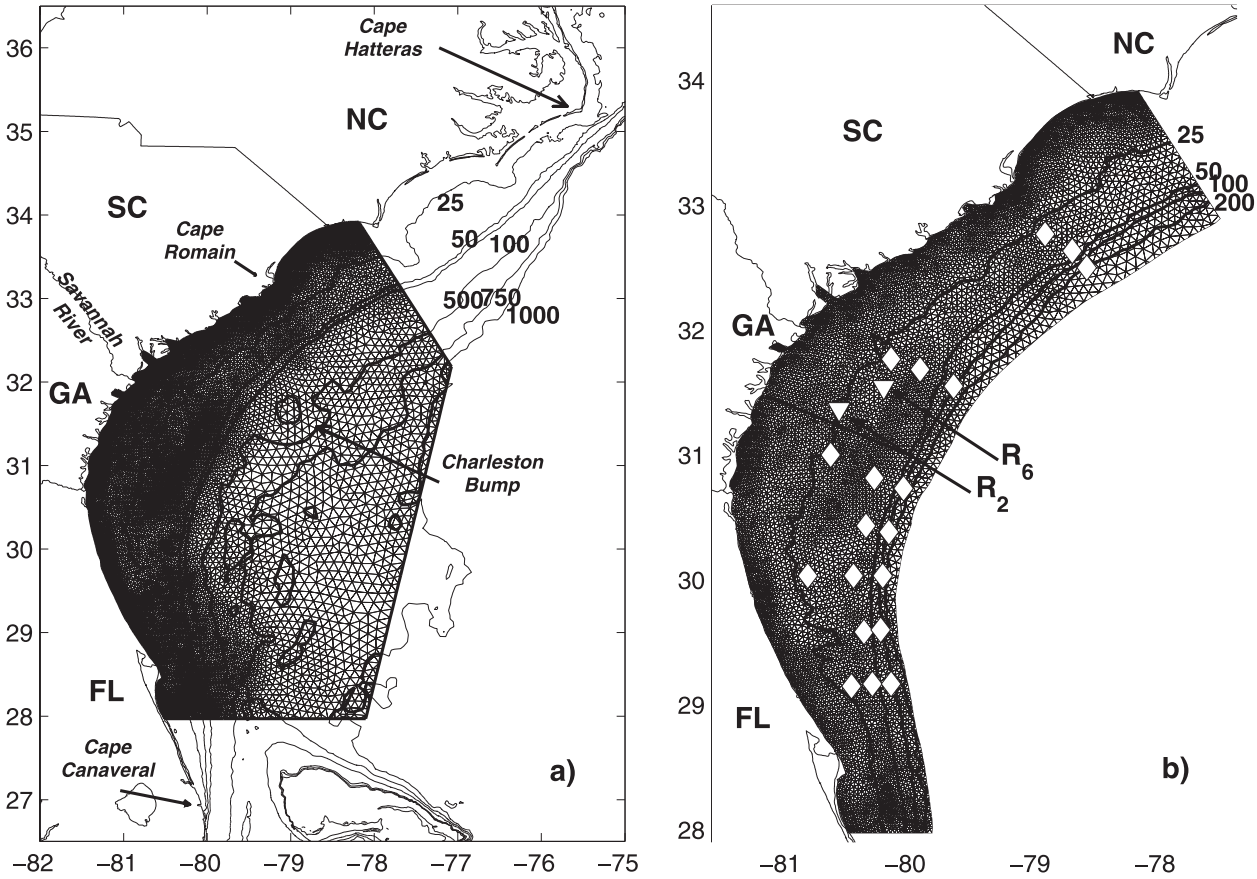

Figure 1. Finite element model climatology domain used for climatological computations. (a) The mesh contains 9606 nodes, 18691 elements. The 25-, 50-, 100-, 500-, 750-, and 1000-m isobaths are shown. (b) The SAB continental shelf region used to display model forcing and response. This is a subregion of the mesh shown in Figure 1a that covers the shelf out to the 300-m isobath. The thick line is the location of the cross-shelf transect discussed later. The locations of two observation stations (R2 and R6) are shown with triangles, and the positions of the Georgia Bight Experiment (GABEX) mooring array are shown with diamonds. The 25-, 50-, 100-, and 200-m isobaths are shown.

SAB (central and south Florida coast) are westward. Summer (June–July) winds are generally along-shelf and poleward over the entire SAB. August appears to be a rapid transition month during which mean winds are weak. Autumn (called "mariner's fall" by *Weber and Blanton* [1980]) spans September-October. The wind stress pattern has shifted to primarily southwestward over the SAB, which is along-shelf in the northern SAB and cross-shelf in the southern SAB.

[5] Over the past several decades, numerous field programs (including GABEX [*Lee and Atkinson*, 1983; *Lee and Pietrafesa*, 1987], GALE [*Blanton et al.*, 1987; *Bane*, 1989], and FLEX [*Werner et al.*, 1993]) have accumulated observations that enable the description of a seasonal circulation climatology. *Lee et al.* [1991] provide schematics of this circulation. The outer shelf (seaward of the 45-m isobath) is dominated by the Gulf Stream, which transports shelf edge waters poleward, except just poleward of a region known as the Charleston Bump which induces a semi-permanent gyre causing occasional equatorward flow along the shelf break [*Bane and Dewar*, 1988]. This is seasonally independent. Mid-shelf flow is generally poleward, presumably driven by an along-shelf pressure gradient induced by an offshore pressure field and supplemented by seasonal wind-driven flow. The inner shelf is influenced primarily by the seasonal wind stress patterns. Drifter paths from *Bumpus* [1973] were analyzed by *Weber and Blanton* [1980] to account for the time difference between drifter release and recovery, with the conclusion that surface flows in the SAB generally follow the seasonal wind regime; offshore in winter (November–February), poleward in summer (June–July), and equatorward in fall (September–October).

[6] There have been several relevant numerical model studies of the SAB. *Kantha et al.* [1982] used a diagnostic transport model solving geostrophic equations to compute annual and seasonal streamfunctions and elevation in the SAB driven by 3-D temperature and salinity (TS) fields from hydrographic archives. *Blumberg and Mellor* [1983] computed winter climatological SAB solutions forced by ideal winds and observed TS fields. These two studies focused on circulation seaward of the shelf break, particularly Gulf Stream transport and the realism of the baroclinically induced flows.

[7] Shelf studies include *Kourafalou et al.* [1984], who used a vertically integrated model limited to the continental

shelf to examine unstratified wintertime velocity and surface elevation shelf response to observed winter wind forcing. Modeled velocities agreed well with observations in the inner and mid-shelf, regions previously established as having a significant wind-driven component. However, outer shelf agreement was less successful due to off-shelf influences on the outer shelf observations. *Lorenzzetti et al.* [1987, 1988] used a two-layer shelf-scale model to examine the shelf upwelling response to summer conditions. They included an along-shelf elevation gradient in conjunction with upwelling-favorable summer winds; both forcings were responsible for the observed mean northward mid-shelf flows. The model-based study of *Werner et al.* [1993] examined the SAB fall shelf response to tides, periodic winds, idealized density fronts, and along-shelf pressure gradients. The main result was that during this season, the wind field is generally downwelling-favorable and responsible for the equatorward flows observed. The along-shelf pressure gradient produced a similar response to that of *Lorenzzetti et al.* [1988], but during fall, the wind-driven equatorward flows dominate the inner and mid-shelf.

[8] To our knowledge, there are no model-based climatologies of the SAB shelf or Georgia coastal region that include a 3-D hydrographic component. However, similar model-based climatologies have been established in other geographical regions using techniques similar to those used herein (see, e.g., *Naimie et al.* [1994] (Georges Bank/Gulf of Maine), *Han et al.* [1997] (Scotian Shelf), *Foreman et al.* [2000] (Vancouver Island), *Naimie et al.* [2001] (Yellow Sea), and *Hannah et al.* [2001] (Scotian Shelf)).

[9] In this study, we combine updated hydrographic observations and the Comprehensive Ocean-Atmosphere Data Set (COADS) wind fields to derive diagnostic density- and wind-driven model solutions in the SAB on a monthly basis. We use a linear, shallow-water, 3-D finite element model formulated in the frequency domain, forced by specified elevation on open water boundaries, imposed internal density variation, and surface momentum flux. Objective analysis is used to map hydrographic observations onto the model domain. We focus on the continental shelf region, although the model domain extend well beyond the shelf limits. This represents an extension of previous modeling efforts in the SAB to 3-D physics that include climatological, objectively derived mass fields.

[10] We are particularly interested in the shelf response in the region of an observation program centered around a set of mid-shelf towers which are the focus of a limited-area synoptic observation system [*Seim*, 2000]. The towers provide part of the observational data set for a shelf-scale forecasting effort using assimilating versions of the model described herein. The monthly mass and flow fields provide one version of best-prior-estimates of the circulation and mass field upon which to base a misfit between model and observations. Assuming a lack of more up-to-date hydrographic information to use as a model initial condition, climatology might be the best information available.

2. Models, Domains, and Boundary Conditions

[11] We use the frequency-domain model FUNDY5SP [*Lynch and Werner*, 1987] with spherical-polar extensions [*Greenberg et al.*, 1998] to compute solutions to the monthly climatological wind stress and TS distributions (described below). FUNDY5SP solves the linearized, harmonic-in-time shallow-water wave equation, subject to surface wind stress, specified elevation or geostrophic outflow on the open boundary, and baroclinic pressure gradients associated with internal density structure, with hydrostatic and Boussinesq assumptions. The vertical eddy viscosity (mixing) is externally specified. The model solutions in this context are the zero-frequency diagnostic response in the region to the wind stress and density gradients.

[12] Two nested model domains are used. We compute the barotropic response (not shown) to the monthly wind stress fields on a large-scale domain that includes the entire North Atlantic west of 60°W. This domain contains 31435 nodes and 58,369 elements, and the only open water boundary is along the longitude 60°W where the elevation is specified to be zero. The vertical discretization uses 21 unequally spaced nodes, with higher resolution in the surface and bottom layers. These model wind solutions are used to obtain the open water boundary elevations for the regional higher-resolution domain on which the climatological solutions are computed.

[13] The second finite element domain, on which the regional (SAB) climatological solutions are computed, is of higher resolution and contains 9606 nodes and 18,691 elements (Figure 1). The domain extends from the coast offshore to about the 1000-m isobath. The elevation on the eastern and northern open water boundaries is specified. A geostrophic outflow condition is specified on the southern boundary [*Naimie and Lynch*, 1993], in which neither the elevation nor transport are known, but it is assumed that a geostrophic balance exists between the two along this boundary. The vertical discretization uses 21 unequally spaced nodes. This domain is subsequently referred to as the climatology domain.

[14] We do not explicitly include tides in this study except for estimating the magnitude and structure of the vertical eddy viscosity and bottom stress. Tidal solutions in the SAB are being investigated separately. The tidal environment in the SAB is a semi-diurnal (primarily M_2) co-oscillation with the North Atlantic deep ocean tide, with significant amplification occurring along the widest part of the continental shelf (off Georgia). The tidal velocity ellipse major axis is generally oriented cross-shelf, with a minor axis length about half that of the major axis length [e.g., *Redfield*, 1958; *Clarke and Battisti*, 1981; *Werner et al.*, 1993]. The tidal Eulerian residual velocity is weak, with shelf break flow toward the equator, and poleward near-shore flow at about 0.01 ms^{-1} [*Werner et al.*, 1993].

[15] The contribution of the tides to the total vertical mixing and bottom stress is included by specifying the eddy viscosity computed with a fully nonlinear, time-dependent 3-D model ([*Lynch and Werner*, 1991; *Lynch et al.*, 1996]) driven by M_2 tidal elevations on the open water boundary, using the same climatology domain described above. This model includes advanced turbulence closure through *Mellor and Yamada* [1982]. The model is spun up over 10 M_2 tidal periods, and the 3-D vertical eddy viscosities $N_z(x, y, z)$ and root-mean-square bottom speed $u_{b,rms}$ are averaged over the last period. The tidally averaged vertical mixing coefficient and bottom speed are subsequently input into the linear

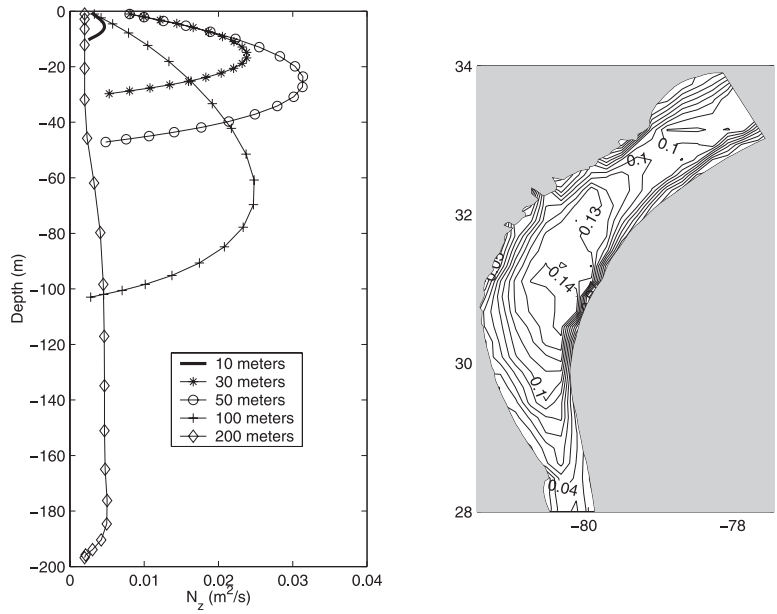

Figure 2. (left) Profiles of vertical eddy viscosity N_z ($m^2\ s^{-1}$) generated by a tidally driven numerical model and specified as the vertical mixing parameterization on the steady-state model FUNDY5SP. The profiles are taken along the transect shown in Figure 1. (right) RMS M_2 bottom speed ($m\ s^{-1}$) used to compute the linearized bottom slip coefficient A_k.

model to more realistically reflect the vertical mixing and bottom stress environment. The linearized bottom stress coefficient A_k is then expressed as $A_k = c_d u_{b,rms}$ where c_d is a drag coefficient (0.005). A minimum A_k of 5×10^{-5} m s^{-1} is prescribed.

[16] Figure 2 shows the spatial distribution of $u_{b,rms}$. The maximum M_2 tidal bottom speeds are greatest (>0.1 m s^{-1}) in the mid-shelf region off the Georgia coast (the widest part of the shelf), and taper off in both the along-shelf and cross-shelf directions. Figure 2 also shows a sequence of profiles of N_z along the cross-shelf transect shown in Figure 1. Mid-shelf maxima reach 0.03 $m^2\ s^{-1}$ at midwater column depths. These values are consistent with the levels of tidal mixing derived from ADCP observations in the region (H. Seim, personal communication, 2002). The profiles shown represent the background level of vertical mixing due to the main tide (M_2) over the tidal cycle and for this study is presumed independent of month.

[17] For the wind-driven computations, the monthly COADS wind velocities are converted to stress via *Large and Pond* [1981] and applied to the model surface layer. The elevation along the northern and eastern boundaries of the climatology domain is specified by computing the surface elevation response on the large-scale domain, driven by the monthly COADS wind stresses, and sampling the large-scale solutions at the climatology domain boundary node locations.

[18] For the baroclinic solutions, the steric elevation along the northern and eastern boundary is computed directly from the derived monthly mass fields. The elevation is computed to compensate for the baroclinic flow normal to the boundary at the bottom, as by *Naimie et al.* [1994] and *Hannah et al.* [2001]. The baroclinic pressure gradients are evaluated on level surfaces and interpolated onto the model's vertical sigma-coordinate grid. The following level surfaces are used, onto which the temperature and salinity fields are interpolated: 0, 3, 6, 9, 12, 20, 40, 60, 80, 100, 150, 200, 250, 300, 350, 400, 450, 500, 600, 700, 800 m. The elevation in the northwest corner of the domain is (arbitrarily) set to zero and pressure gradients evaluated relative to this value.

3. Data Sources and Processing

3.1. Surface Winds

[19] Ten-meter east and north wind speeds are acquired from the COADS data set [*Woodruff et al.*, 1998]. The COADS data sets are comprised of in situ observations of wind speed, atmospheric pressure, water/air temperature, etc., mainly from ships of opportunity, that have been acquired, quality-controlled, and summarized statistically on a monthly basis on 1° squares. These monthly summary groups (MSGs) from the years 1975–1997 are taken for the northwest Atlantic region and split into months. The resulting data are block averaged onto a 1° × 1° grid (using data for which the sample size is greater than 20), smoothed with a nine-point Laplacian filter, and then linearly interpolated onto both the large-scale and climatology model grids for computations.

3.2. Hydrography

[20] Temperature and salinity (TS) profiles for the region were acquired from the National Oceanographic Data Center (NODC) for the SAB region. Figure 3 shows NODC profile locations available by month for the region. Our "quality control" method is as follows: profiles whose bottom depth is less than 400 m are manually inspected for TS values grossly out of range, based on the established SAB shelf climatology of *Atkinson et al.* [1983]; for data whose bottom depth is greater than 400 m, TS diagrams

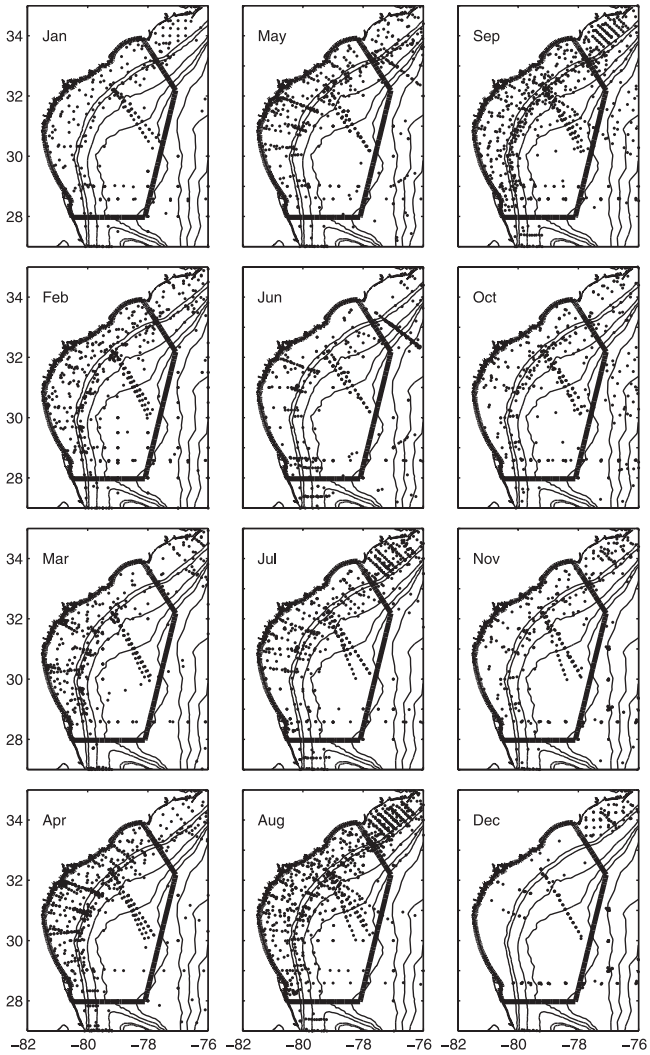

Figure 3. NODC station locations in the SAB by month. The data for each month spans 50 days centered on day 15. For example, January data are from the range 20 December through 10 February. The climatology domain boundary is also shown.

(Figure 4) are constructed on half-degree squares and TS pairs that deviate by ±2 standard deviations from the computed TS curves are eliminated.

[21] The spatial distribution of the TS curves in the SAB is presented in Figure 4. The previously observed [*Emery and Dewar*, 1982] consistent character of TS properties in the off-shelf region is noted. The upper water column variability of the Gulf Stream off-shelf position is evident along the shelf break, particularly downstream of the Charleston Bump. Farther off-shelf, the TS relationship is tighter. However, the shelf region exhibits no well-defined TS relationship, indicating that it is critical to observe both temperature and salinity to define the shelf mass field.

[22] The resulting available data are presented in Figures 3 and 5. There are about 45,000 TS pairs from 5000 NODC profiles available for this region, spanning 1950 to 1999. For the purposes of our optimal interpolation of the available data to produce monthly TS fields, we have gathered the data into 50 day blocks, centered about day 15 of each month (for example, for the January TS field estimates data are averaged across the period 20 December to 10 February). Even with this procedure, significant data gaps in both space and time are apparent in the monthly data; note particularly shelf gaps in June, October, and December. All months exhibit a significant gap near 79°W, 30°N. However, our primary focus is on shelf climatology and the resulting shelf temporal and spatial coverage is largely adequate. We therefore do not focus further on the off-shelf characteristics of the forcing or the model solutions.

3.3. Objective Analysis

[23] In order to compute monthly climatological solutions for elevation and velocity, the TS fields defined by the TS data must be mapped onto the model domain, both horizontally and vertically. We use an objective analysis (OA) technique [*Bretherton et al.*, 1976] to map the spatially and temporally irregular TS data onto a specific set of coordinates (the model nodes). This method requires the definition of a set of correlation scales at each model node, from which the method computes a set of nearest neighbors and interpolation weights. The general OA method is 4-D (x,y,z,t); however, owing to the irregular temporal distribution of the NODC data in time (see Figure 5), it is difficult to choose a time per month about which to center the temporal average. We have therefore eliminated the temporal dependence by lumping all data for a given month (the 50-day window previously described) to the month center. Our OA uses 50 nearest neighbors and with correlation scales that are largely isotropic; 100 km on the shelf and offshore for both the cross- and along-isobath directions, and 100 km cross-isobath and 200 km along-isobath along the shelf break (100 m < bottom depth < 500 m). The scales vary smoothly over these ranges according to the steepness of the bottom topography. We have used a smoothed version of the bathymetry for the scale definition to avoid local abrupt changes in the correlation scale directions. The vertical scales are: 10 m for depths <100 m, 25 m for depths between 100 m and 500 m, and 50 m deeper than 500 m. Using the above scales, the monthly TS fields are interpolated onto the climatology domain level surfaces. Finally, the data contain density inversions, and so each vertical TS profile is adjusted to remove static instabilities using a vertical mixing model based on work by *Mellor and Yamada* [1982].

4. Monthly Forcing and Response

[24] Two sets of monthly solutions are computed from the COADS wind fields. First, the wind stress is applied to the large-scale domain that covers the western North Atlantic ocean. This is done solely to determine the elevation along the climatology domain boundary that results from far-field wind setup effects on the boundary. Otherwise the elevation on the climatology domain boundaries would be set to zero. Second, for the climatology domain, we compute the monthly mean wind response with elevation boundary conditions as just described and with the monthly COADS wind stresses. Results on the large-scale domain are not

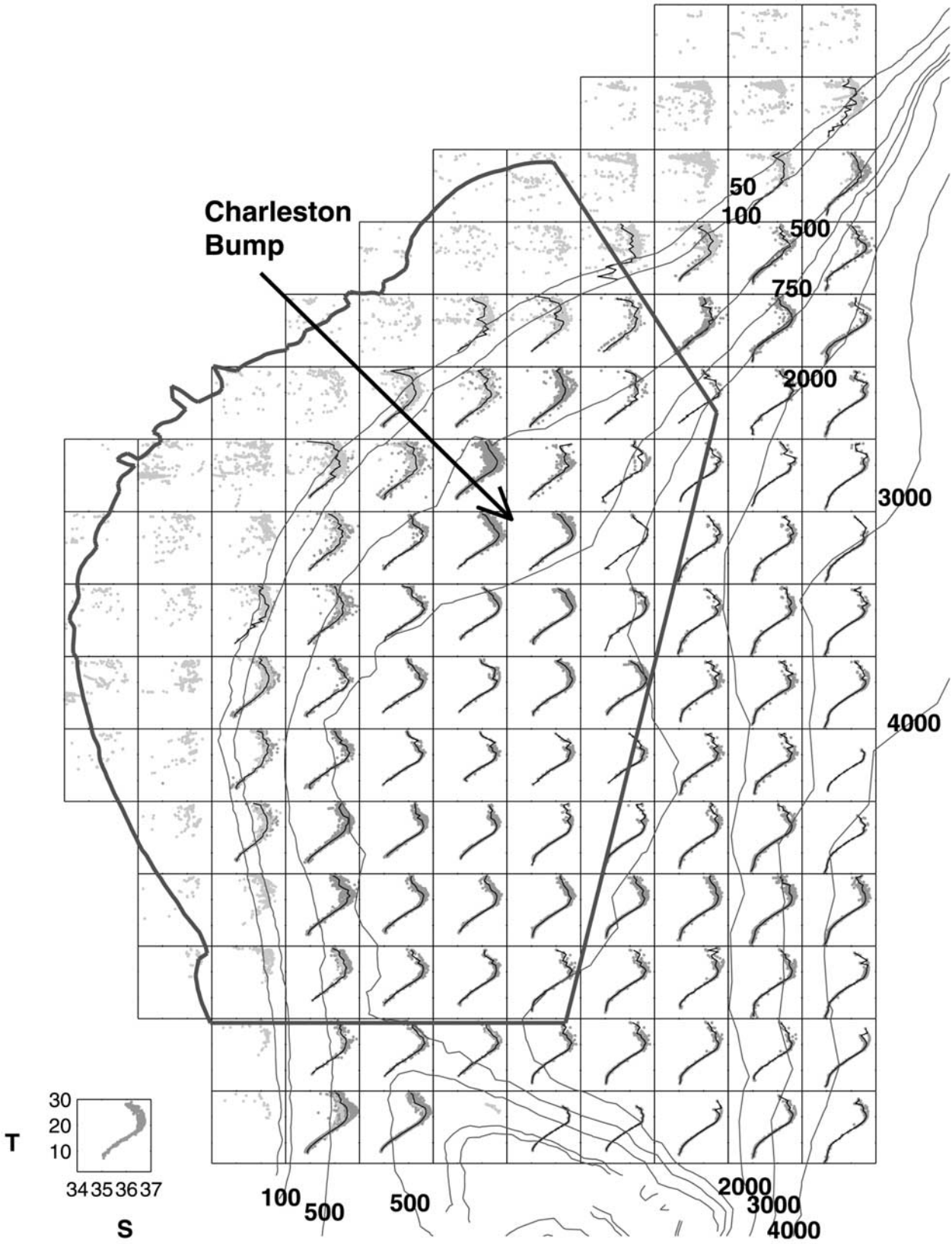

Figure 4. TS diagram distribution. Salinity is on the abscissa; temperature is on the ordinate. The TS curve axis scales for all squares are shown with the separate diagram in the lower-left. Shelf data (<400 m) are in green; deeper water (>400 m) data are in red. For the deep squares, the average TS curve is drawn in black. The 50-, 100-, 500-, 750-, 1000-, 2000-, 3000-, and 4000-m isobaths are shown. See color version of this figure at back of this issue.

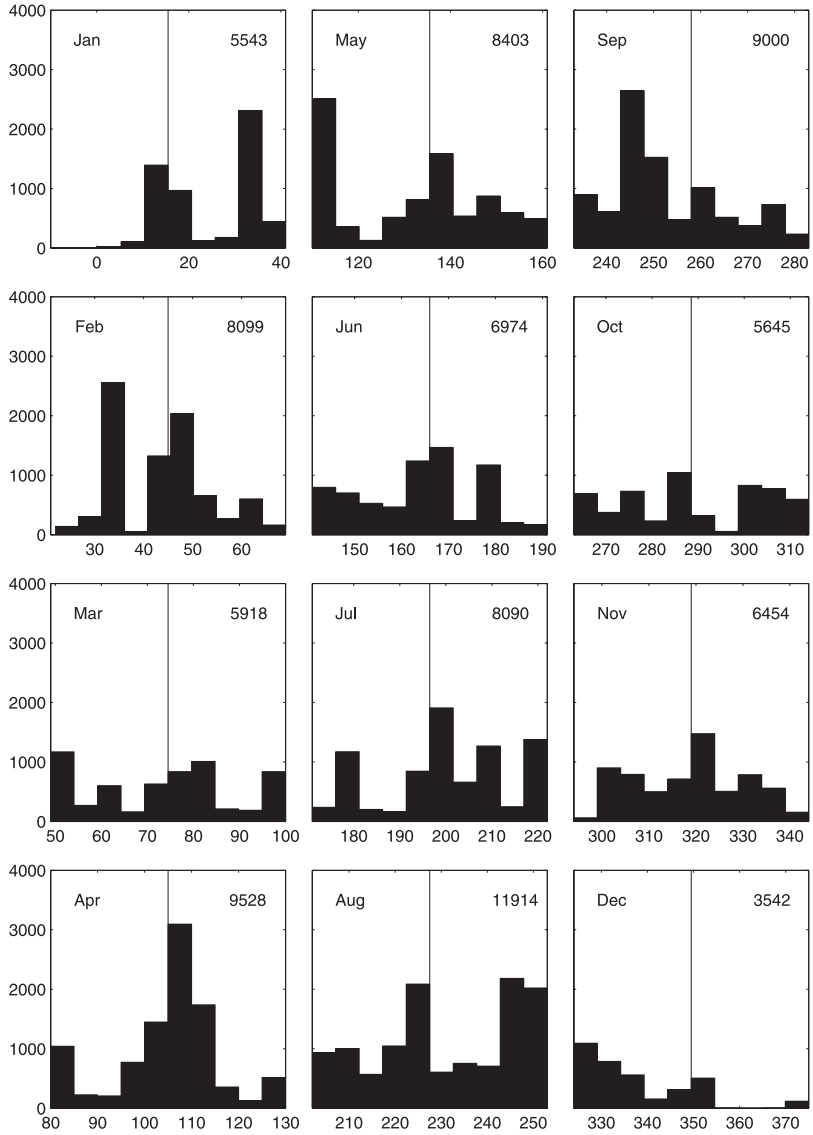

Figure 5. NODC monthly temporal distribution. The middle of each month is marked by the vertical line, and the abscissa is in Julian days. The numbers in the upper right of each panel are the total TS pairs available for the month.

shown. The response on the climatology domain due to the objectively analyzed monthly mass fields is computed separately. Since the model is linear, these solution sets can be added together to obtain the total flow for each month.

[25] For the climatological forcing and response, we illustrate important differences between monthly regimes with results for selected months: January, April, July, and October. We describe below the general meteorological and oceanic forcings, restricting our attention to the shelf region shoreward of the 300-m isobath. Display of horizontal fields of both the forcing and model response is shown on the shelf region as in Figure 1b. Observations of coincident TS pairs are spatially and temporarily sparse in the offshore region. The resulting TS objective analysis reveals the basic expected offshore density structure of the Gulf Stream region, but the transport is generally too weak, and some months (December and January, particularly) do not contain enough data to define the expected cross-stream structure.

4.1. COADS Forcing

[26] Figure 6 shows the COADS surface wind velocity and surface atmospheric pressure for the representative months for a portion of the western North Atlantic that includes the Caribbean Sea, SAB, the lower MAB and extending offshore to Bermuda (66°W). The large perspective reveals the strong and persistent westward trade winds below about 27°N. The following wind field climatology is consistent with that of *Weber and Blanton* [1980] and *Blanton et al.* [1985]. Winter conditions (January) show the high-pressure ridge in place extending across the mid-latitudes, and steering the mean winds cross-shelf in most of the MAB and SAB. Winds are generally offshore with increased strength toward the MAB.

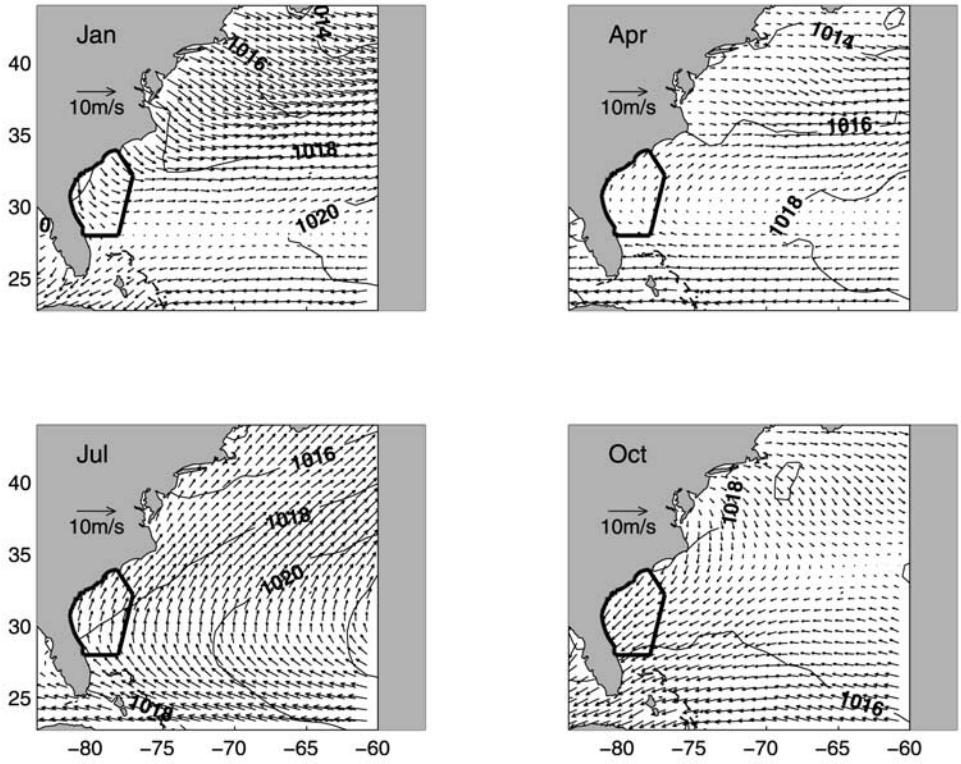

Figure 6. Monthly COADS surface wind velocity (m s^{-1}) and atmospheric pressure (mbar) for a portion of the western North Atlantic. The climatology domain boundary is included.

[27] Spring (April) is a transition period where the strength of the high-pressure region has decreased, and the ridge no longer extends westward into the SAB. The corresponding SAB wind field is largely variable and weakly poleward and along-shelf in the SAB region and generally weak and offshore over the lower MAB. From May to July (summer), the offshore high strengthens with winds strengthening in response. The Bermuda high dominates the region, with winds largely upwelling favorable, being along-shelf and poleward along the entire eastern U.S. coast. In August (not shown), the high pressure weakens with weak winds beginning to shift counterclockwise from the along-shelf poleward upwelling-favorable summer regime toward the along-shore equatorward, downwelling-favorable fall. Fall (October) shows along-shelf equatorward winds in the upper SAB, and onshore winds along the Florida coast. The high-pressure ridge has returned.

4.2. Hydrography

[28] Surface and bottom salinities and temperatures from the monthly objective analysis are shown in Figures 7 and 8. Winter (December-March) shelf surface temperatures are generally uniform along isobath, ranging from shelf edge temperatures of about 20°C to 10°C along the upper SAB coast. The Florida coast experiences an along-shelf temperature gradient of about 6°C. Salinity ranges from 36.5 to 33, with isohalines largely parallel to isobaths. In spring, shelf temperatures increase only marginally along the shelf break and by 5–10°C along the coast, causing the strong cross-shelf temperature gradient to be greatly reduced. Salinity increases slightly along the shelf break and decreases by about 1 along the coast. River discharge peaks in late March to early April [*Atkinson et al.*, 1983], and the offshore extent of the fresher water is evident along the Georgia coast. The surface salinity minimum of 32 occurs nearshore just south of the Savannah River entrance. Surface waters warm rapidly, and by July, surface temperature is relatively uniform at 28°C. Surface salinity is also more uniform at 35–36, with river discharge still evident near 32°N. Cooling of shelf waters occurs rapidly between September (not shown) and October. October isotherms lie along-shelf with a cross-shelf difference of about 4°C.

[29] Bottom temperatures and salinities are shown in Figure 8. January bottom temperatures are generally along-shelf, except along the north Florida coast, with a strong cross-shelf difference of 10–12°C. Cooler shelf break waters are evident, with a bottom temperature maximum near 20°C occurring along the 100-m isobath. April bottom waters warm significantly by 6–8°C. By July, bottom temperatures reach their maximum near the coast, and upwelling of cooler water along the shelf break is evident. Unlike the July surface temperatures, the bottom temperature exhibits strong cross-shelf structure and is relatively constant along-shelf. October bottom temperatures range from about 21–25°C. Bottom salinity is generally along-shelf, with shelf break salinity constant at 36, and cross-shelf temperature differences ranging from 5°C in January to 2°C in July. In all months the cooler, more saline shelf break water is evident.

[30] The surface density (σ_t) is shown in Figure 9 (top). January and October results indicate an along-shelf density

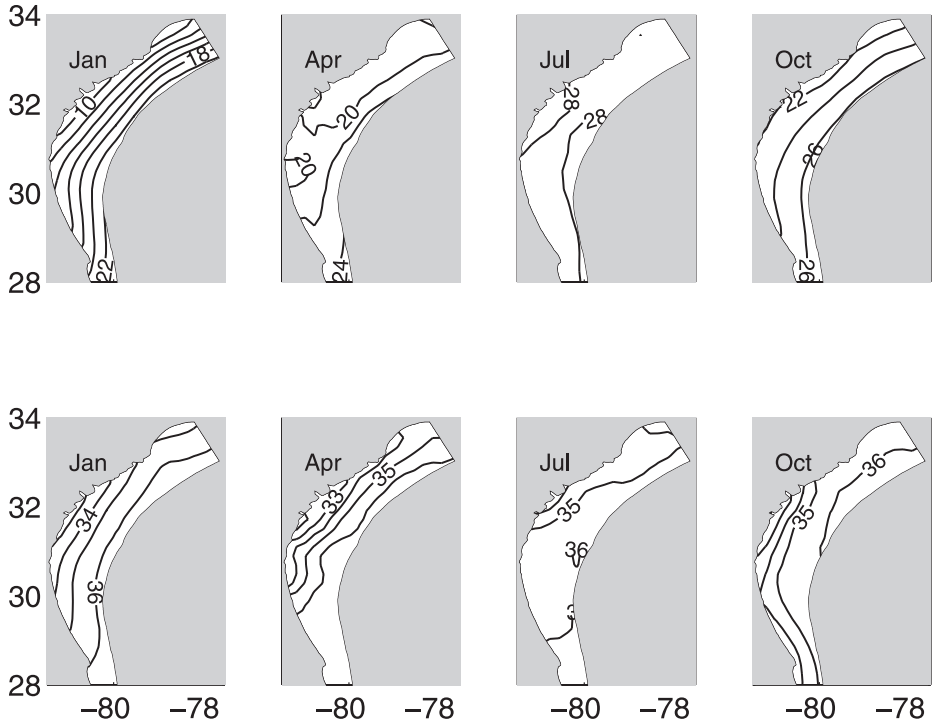

Figure 7. SAB monthly (top panel) surface temperature and (bottom panel) surface salinity objective analysis.

difference of about 2 σ_t, with denser water in the northern part of the bight. The surface density gradient in April is mostly cross-shelf, with a small along-shelf component. July surface density is relatively constant with a small (1 σ_t) cross-shelf gradient in the middle of the domain.

[31] Figure 9 (bottom) shows the density difference between the surface and bottom (σ_t^{s-b}). This difference is an indication of the strength of stratification, with more negative values indicating stronger stability of the water column. The bulk of the SAB shelf in January (winter) is

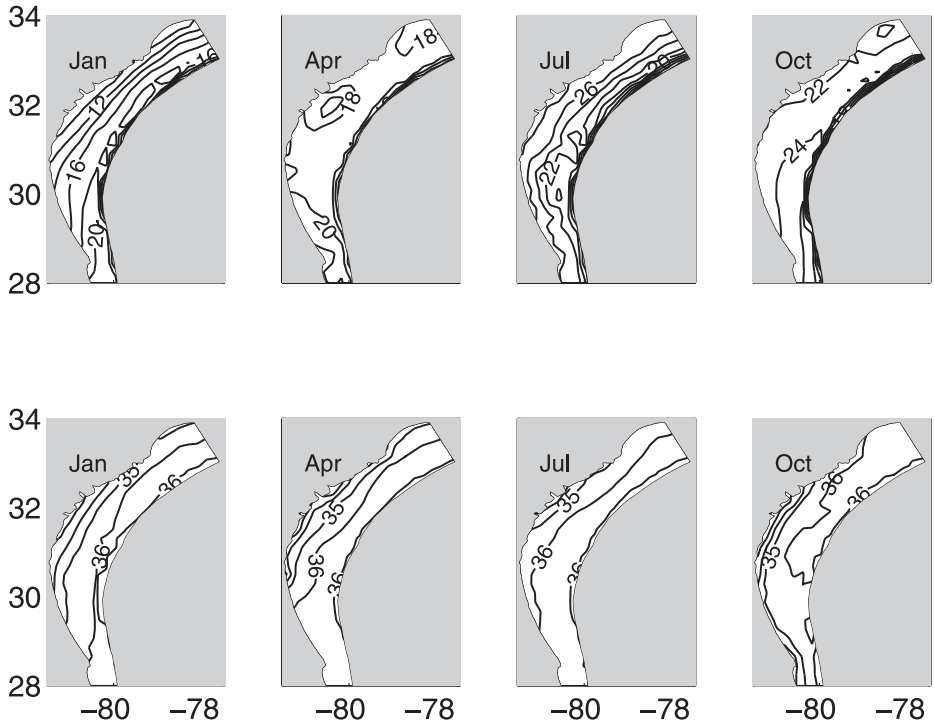

Figure 8. SAB monthly (top panel) bottom temperature and (bottom panel) bottom salinity objective analysis.

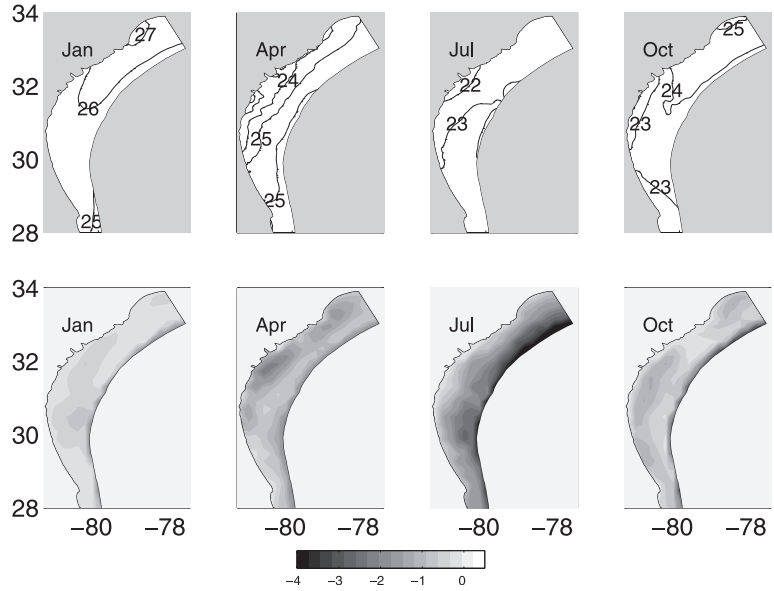

Figure 9. (top) SAB monthly surface σ_t. (bottom) SAB monthly top-bottom σ_t difference. More negative values indicate stronger stratification, and zero indicates neutral stability.

marginally stable with $\sigma_t^{s-b} > -0.5$, except along the shelf break where the warmer Gulf Stream water in the upper layers imposes slight thermal stratification. By April, the fresher water discharge from the Savannah River and surrounding rivers provides a less dense layer forming a strongly stratified region (-2 σ_t difference) at 32°N. The remainder of the shelf is also stratified. There is a general tendency for the mid-shelf to be stratified to a weaker extent than the inner and outer shelf. By July, the stratification is strong throughout the shelf, aligning along isobath and strongest at the shelf break. The strength of the stratification decreases by October with the near-shore inner shelf becoming weakly unstratified. In all months, the shelf break is permanently stratified.

[32] Figure 10 shows the cross-shelf structure of the temperature, salinity and density fields for January, April, July, and October, along the transect shown in Figure 1b. In January, shelf waters are largely weakly stratified; temperature and salinity are well-mixed in the upper half of the water column, in the inner and mid-shelf. Warmer, saltier waters are evident in the lower part of the water column, in the mid- to outer shelf. The resulting σ_t shows a mid-shelf denser pool (>26 σ_t units). Freshwater river discharge from local rivers peaks in March–April [*Atkinson et al.*, 1983], apparent in the April hydrography. The cross-shelf temperature difference is about 4°C; the inner shelf has started to more strongly stratify. The fresher water front extends to about the 30-m isobath. As the summer progresses, strong stratification develops throughout all but the near-coast region of the shelf (July is representative of July–October); salinity is largely constant, and the temperature is strongly stratified, except in the mid-shelf upper 20 m of the water column. Surface temperatures are >28°C, with the upwelling of cooler (<26°C) waters at the shelf break. The increased storm activity in the fall begins (along with decreasing air temperature) to break down the stratification that developed over the summer. By October, the upper 10–20 m have become well mixed but lower depths retain some stratification, particularly in salinity.

[33] Along this transect, the vertically integrated cross-shelf density gradient $R_x = \int_{-h}^{0} \partial\rho/\partial x \, dz$ is positive inshore and negative in the outer shelf. The sign change (where $R_x = 0$) occurs at about mid-shelf in January, moves offshore in April and July, and moves back to mid-shelf by October.

4.3. Monthly Response to Wind Forcing

[34] The model was run on the large-scale domain using the monthly wind stress fields (shown in Figure 6) to compute the large-scale response to the wind fields (not shown). The surface elevation for the climatology domain is extracted from the monthly large-scale solutions along the eastern and northern open water boundaries. The solutions to the wind fields (for the SAB shelf region) with the imposed boundary elevation from the large-scale domain are shown in Figure 11a where the surface elevation and surface velocity are given. January winds have a large cross-shelf component in the northern SAB, and turn more along-shelf toward the south. The along-shelf flow is equatorward ranging from 0.05 m s^{-1} in the inner shelf to near zero m s^{-1} on the widest part of the shelf. The Ekman-driven elevation setup is maximum along the Georgia coast (at about 31°N) at 0.025 m. April winds are significantly weaker and poleward. The resulting wind-driven flow is very weak; the flow is confined to the inner shelf where velocities are less than 0.02 m s^{-1} and the elevation response is flat. By July, the summer winds have strengthened and the shelf flow is poleward, with the associated coastal elevation setdown most negative in the southern SAB. This is effectively the reverse of the January (wintertime) situation. The wintertime atmospheric pattern is re-established by October, where the winds are along-shelf in the northern SAB and essentially onshore along the north Florida coast. The flow is equatorward at 0.025 m s^{-1}. Coastal elevations are highest in the southern SAB. In all months for which the along-shelf flow is firmly established, the elevation response generally follows depth contours. Additionally, the steepest elevation response is along the north Florida coast, where the shelf is narrowest.

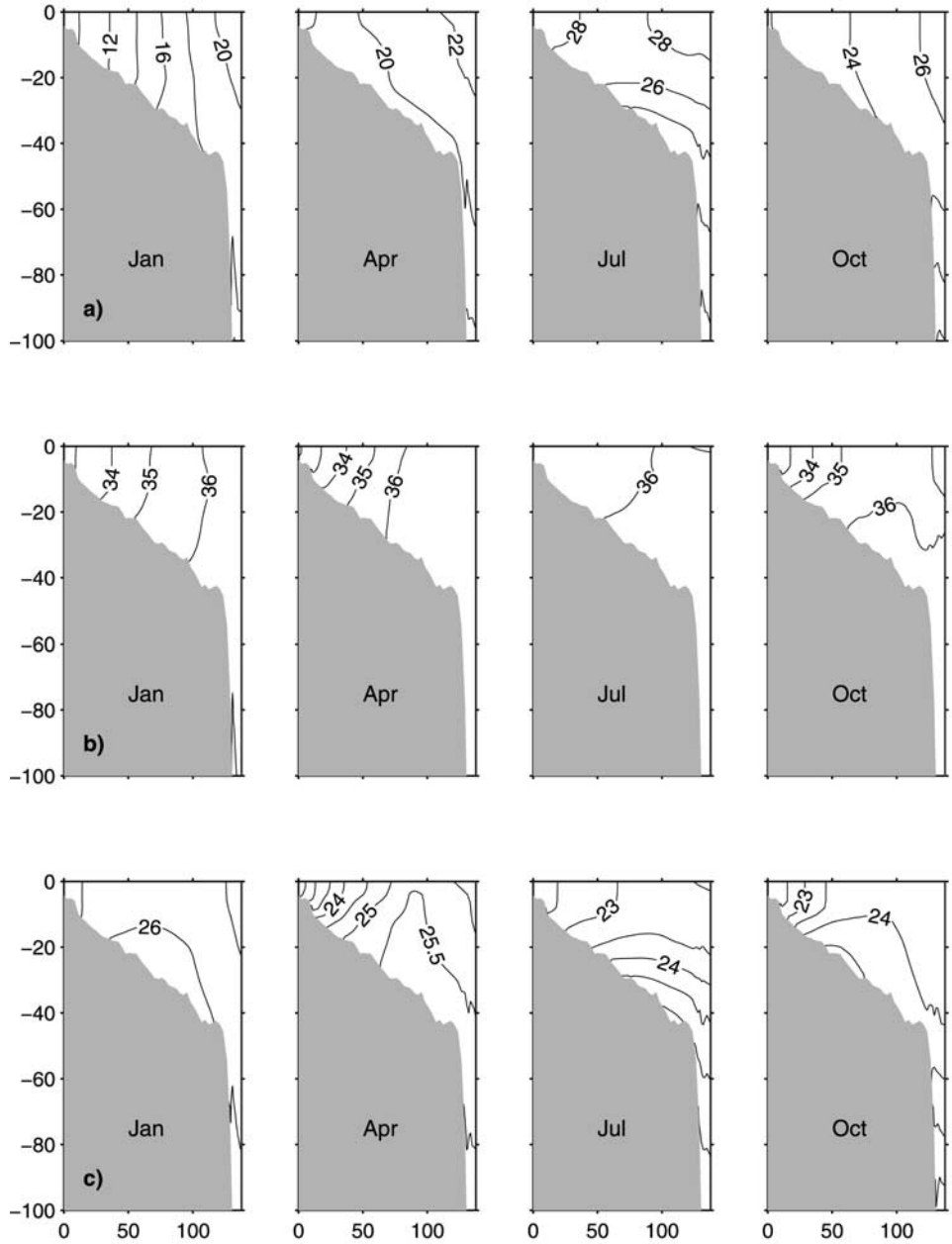

Figure 10. Monthly (a) temperature, (b) salinity, and (c) σ_t along cross-shelf transect shown in Figure 1. The contour intervals are 2°C, 1 PSU, and 0.5 σ_t units, respectively.

[35] Figure 12 shows the January and July wind-driven solutions sampled along the 70-m isobath. The vertically averaged velocity has been subtracted from the total velocity. During January, downwelling winds drive surface Ekman flow onshore with surface elevation setup at the coast and compensating offshore flow in the lower water column. This is a persistent feature along the length of the shelf with the normal-component flow decreasing in intensity toward the north. The zero normal flow line is at about mid-depth (≈35 m) along the entire shelf break. The vertical velocity along the shelf break is negative at about -5×10^{-5} m s^{-1} (not shown). The reverse (upwelling) scenario occurs in July. In all cases, the larger response is concentrated at the narrowest part of the shelf. In the summertime upwelling numerical experiments of *Lorenzzetti et al.* [1987], a similar pattern was found despite the along-shelf component of windstress being stronger in the northern SAB.

4.4. Monthly Response to OA Hydrography

[36] The monthly shelf depth-averaged flow and surface elevation responses to the monthly climatological TS distributions are shown in Figure 11b. Recall that this is the diagnostic response to the imposed, data-derived mass field. The presence of the Gulf Stream is evident, where the climatological signal of the jet dominates the response in the southern portion of the SAB shelf. In January, July, and October, the entire shelf flow is poleward, with inner and mid-shelf speeds of 0.01–0.1 m s^{-1}. January flows are the strongest. The surface elevation generally is higher at the

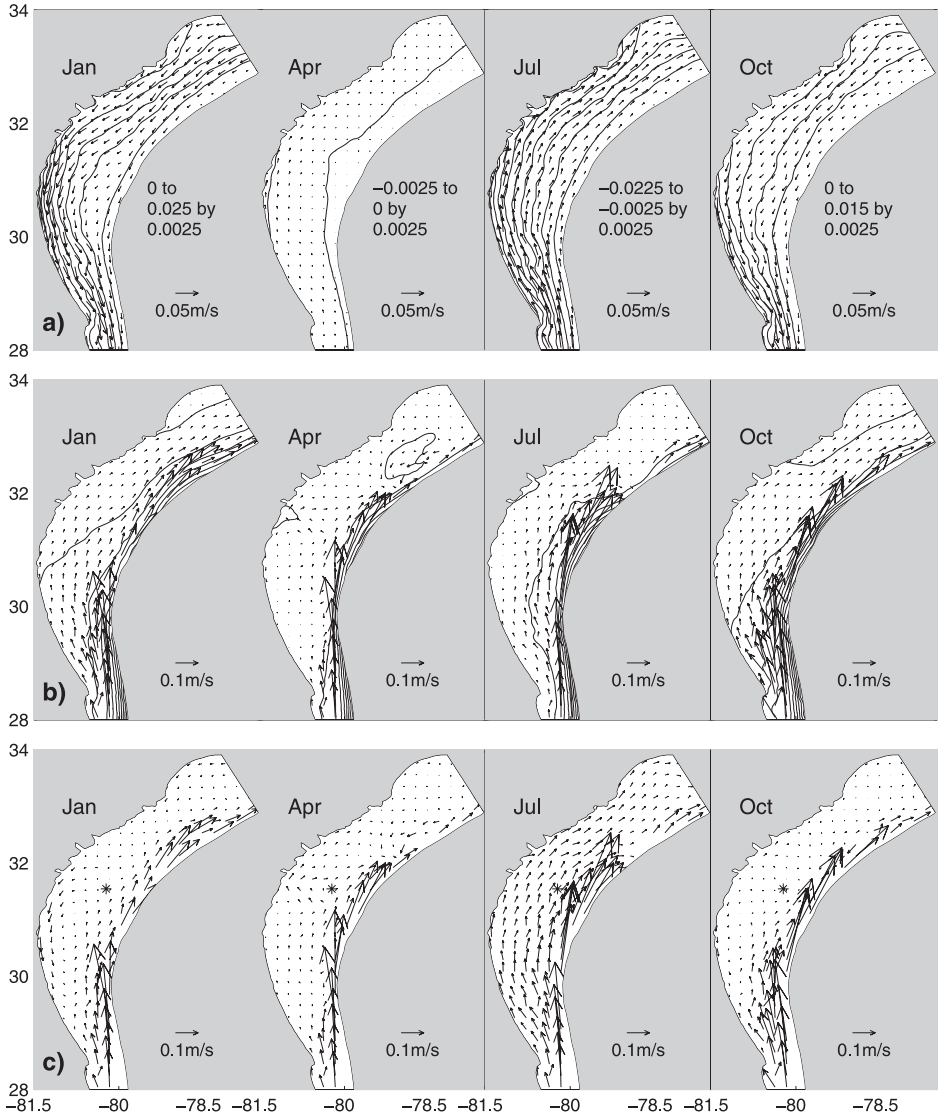

Figure 11. SAB monthly response to forcings. In all cases, velocities exceeding 0.5 m s^{-1} are not shown. The velocity has been interpolated to an equally spaced grid for clarity. (a) Surface elevation and depth-averaged velocity response to the COADS monthly wind fields, with imposed open boundary elevation from large-scale solutions. The elevation range and contour interval are given next to each month. Elevations nearest to zero are at the shelf break. (b) Surface elevation and depth-averaged response to the climatological mass fields. Elevation contours start at 0.025 m near the coast with a contour interval of 0.025 m. Largest elevations are at the shelf break, and the elevation at the northwest corner of the domain is set to 0 m for the density-driven solutions. (c) Combined (wind- plus density-driven) solutions. Elevation is not shown. The R6 tower location is indicated with an asterisk. Note that the vector scale in Figure 11a is 0.05 m s^{-1}, and in Figures 11b and 11c it is 0.1 m s^{-1}.

shelf break than at the coast location, and there is an elevation difference along the shelf break of 0.05–0.15 m. Figure 13 shows the elevation for January along the 70-m isobath.

4.5. Combined Solutions

[37] The separate monthly solutions indicate that the density-driven flow is generally weaker in magnitude than the wind-driven flow in the inner shelf, and of the same magnitude in the mid-shelf. The combined (wind- plus density-driven flow) result (shown in Figure 11c) is that during October and January, there is net equatorward flow in the inner shelf, there is little net flow in the mid-shelf, and there is net poleward flow on the outer shelf. In July the winds are northeastward and thus the wind- and density-driven flows reinforce each other. The net result is that there is shelf-wide poleward flow. Finally, in April the net flow is very weak. In all cases, the effects of the Gulf Stream along the north Florida shelf appear to reach mid-shelf.

4.6. Comparison to Observations

[38] As noted in the introduction, the accumulated current meter observations in the SAB have allowed the characterization of the mean circulation in schematic terms. Among

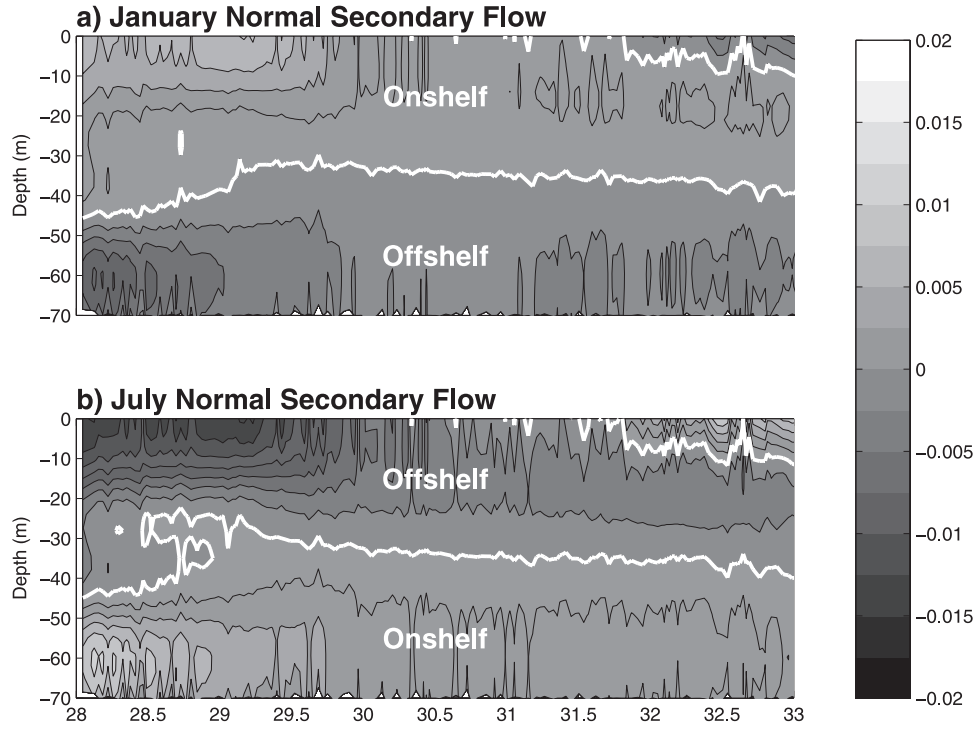

Figure 12. Model wind-driven horizontal velocity (m s^{-1}) normal to the shelf break (along the 70-m isobath) for (a) January and (b) July. The depth-averaged normal velocity has been removed. In the local rotation, flow on shelf is positive. The white lines indicate zero m s^{-1}.

the observation programs in the SAB, the Georgia Bight Experiments (GABEX I [*Lee and Atkinson*, 1983; *Lee et al.*, 1985] and GABEX II [*Lee and Pietrafesa*, 1987]) provide the broadest simultaneous spatial and temporal coverage. These programs occupied a series of cross-shelf transects from about 29°N to Cape Romain, South Carolina, at the locations shown in Figure 1. The off-shelf extent of each transect terminated on the 75-m isobath, and the transects were occupied from 16 February to 2 July, 1980, in GABEX I, and from 1 June to 15 October, 1981, in GABEX II. Our model solutions have been averaged over the same months as the GABEX periods and sampled at the same horizontal positions. The results are shown in Figure 14.

[39] Consistent with the 4-month means provided by *Lee et al.* [1985, see their Figure 7] and *Lee and Pietrafesa* [1987, see their Figure 3], along-shelf flows decrease in strength toward the coast, with surface flows stronger than bottom flows. The presence of the Gulf Stream along the shelf break is evident, including weaker shelf break flows in the northern part of the domain that are consistent with a more variable Gulf Stream frontal position downstream of the Charleston Bump [*Singer et al.*, 1983]. There is also evidence in the model solutions of on-shelf flow with depth on the north Florida shelf in both seasons. Mid-shelf flows are significantly weaker and with less vertical shear. Along-shelf flows in the diagnostic solutions are generally weaker than the observations. The averaged model solution for the GABEX I period shows weaker (and at one station equatorward) shelf break flow around 30°N. This is most likely due to the aliasing of temporal variability into spatial variability in the objective analysis of the TS fields. The same cause may also explain the equatorward flow at the northern shelf break GABEX I station, although we note that persistent equatorward flows in this region are observed [e.g., *Singer et al.*, 1983], associated with seaward Gulf Stream deflection in the region.

[40] Long-term (multi-year) stationary observations of velocity in the SAB have only recently become available. A set of platforms off the Georgia coast has been instrumented with meteorological and oceanographic sensors [*Seim*, 2000]. From this installation an acoustic Doppler current profiler (ADCP) data set (from the R6 tower location shown in Figure 1) and a wind velocity record (from the R2 tower location) are available from the period 01 May 2000 through 30 June 2002. The towers are about 20 km apart. The records were separated into winter and

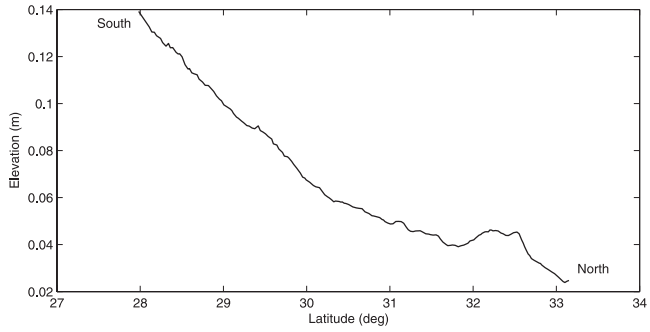

Figure 13. Free-surface elevation along the 70-m isobath for the diagnosis of the January mass field. The resulting along-shelf elevation difference is about −0.12 m in 6° latitude giving an along-shelf slope of -2×10^{-7}.

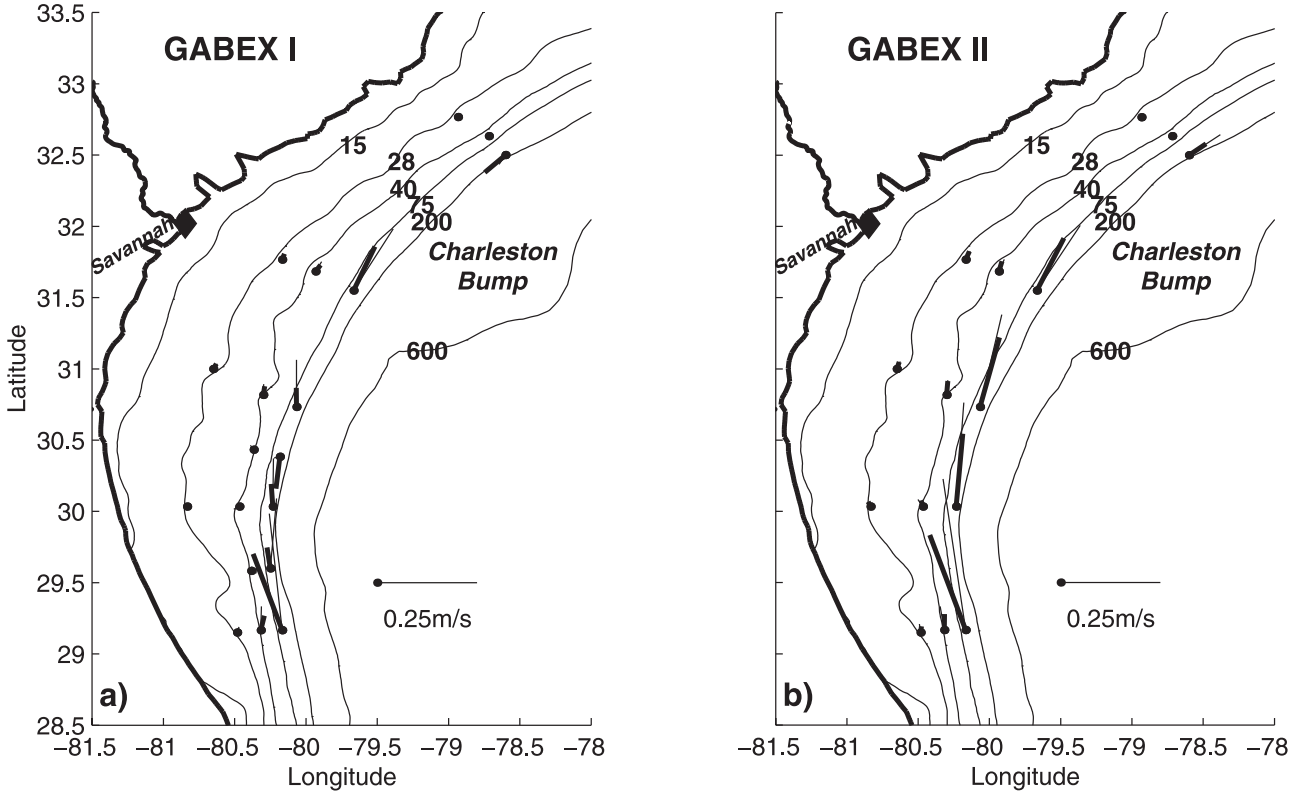

Figure 14. Combined climatological solutions sampled at the (a) GABEX I and (b) GABEX II mooring locations. Upper level (17 m below surface) velocities are shown with thin vectors; lower level (3 m above bottom) are shown with thick vectors. The GABEX moorings shown were stationed at the 28-, 40-, and 75-m isobath. The model bathymetry is not completely coincident with that reported in the GABEX programs.

summer periods that correspond to periods when the COADS wind fields are generally (locally) in the same direction. These periods are December–February when the local winds are generally cross-shelf at the observation location and May–August when the winds have a strong along-shelf (poleward) component. Table 1 compares the along-shelf and cross-shelf winds at the tower location R2 with the COADS winds at the same location. The R2 along-shelf winds are stronger than the climatological (COADS) winds, and both are poleward during summer and equatorward during winter. The cross-shelf component is weaker in the R2 winds; both are onshore (negative) during summer and offshore during winter. There is little difference in the R2 observations between the averaging periods.

[41] The R6 ADCP velocity was low-pass filtered at 40 hours, rotated into along- and cross-shelf (the principal axis is 31° toward east from true north) and averaged over the two periods. The results are shown in Figure 15, for the depth-dependent flow, and the vertical averages are given in Table 2. Poleward flows and offshore flows are positive, and equatorward flows and onshore flows are negative.

[42] The summer vertically averaged along-shelf flows at the R6 tower location are poleward at 0.02–0.03 m s^{-1} for both the model climatology and the two summer periods of observations. This is the result of generally wind-driven flow in the mid-shelf. The cross-shelf component is an order of magnitude smaller. Winter along-shelf flows in the combined model solutions are poleward at about 0.01 m s^{-1}. The observed flow for the first winter period (December 2000 to February 2001) is equatorward, while for the second winter period it is poleward.

[43] The observed cross-shelf flow (left panels in Figure 15) shows a reversal of flow with season. The surface flow is onshore (offshore) and the bottom flow is offshore (onshore) in winter (summer). Although the model cross-shelf flow is very weak (<0.01 m s^{-1}), it exhibits the same flow reversal with season (see also Figure 17 in section 5).

Table 1. Comparison of Mean Wind Velocity (m s^{-1}) at Location of Tower R2[a]

	December–February		May–August	
	CS	LS	CS	LS
COADS	1.94	−0.62	−0.93	1.61
R2,1	1.63	−1.61	−0.51	2.40
R2,2	1.46	−1.01	−0.35	1.89

[a]The data have been rotated into cross-shelf (CS) and along-shelf (LS) orientation of the R6 station (31° clockwise from true north). Top row is from the COADS monthly summary groups over the years 1975–1999. Middle row is from the tower R2 meteorological station over the periods December through February for 2000–2001 and May through August 2000. Bottom row is from the tower R2 meteorological station over the periods December through February for 2001–2002 and May through August 2001. For the along-shelf values, poleward flow is positive and equatorward flow is negative. For the cross-shelf values, offshore flow is positive and onshore flow is negative.

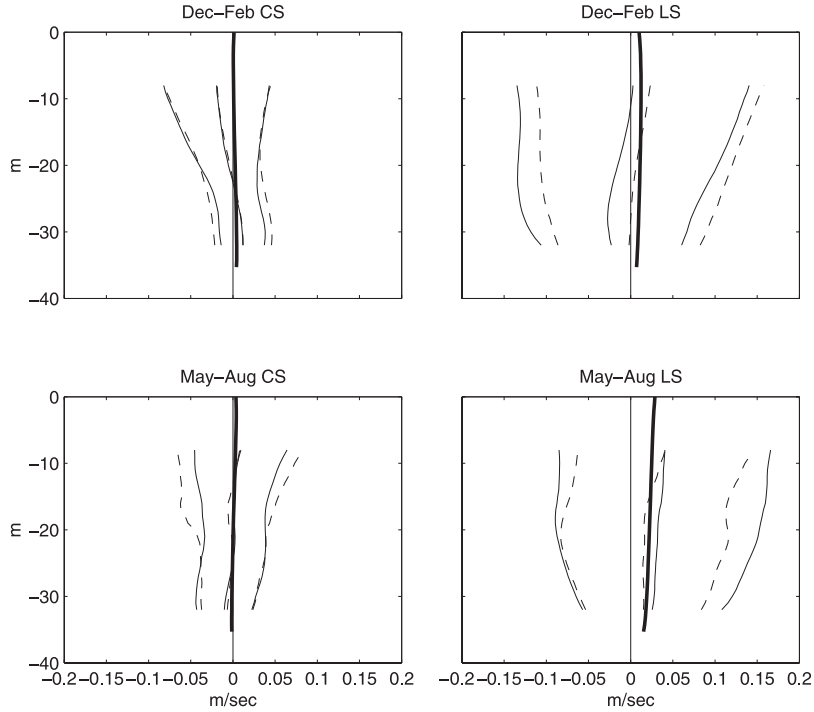

Figure 15. Comparison of ADCP and climatology velocity profiles. "Seasonal" and averaged ADCP velocity profiles from tower R6 are shown. Data have been rotated into along-shelf (right) and cross-shelf (left) directions. (top) The winter season is over the periods December through February for 2000–2001 (thin solid line) and 2001–02 (thin dashed line). (bottom) Summer is defined as May through August for 2000 (thin solid line) and 2001 (thin dashed line). Thick lines are the model solutions; thin lines are the ADCP averaged profiles with one standard deviation. For the along-shelf panels, poleward flow is positive and equatorward flow is negative. For the cross-shelf panels, offshore flow is positive and onshore flow is negative.

[44] The winter along-shelf flow at R6 shows an interesting difference between the two winter time averaging periods. Based on the combined model solutions, R6 is situated near the edge of the "no net flow" region. The observed mean flow for the first winter period is actually equatorward and highly sheared. This is contrary to the model solution, but consistent with the winds during this period. However, the along-shelf current speed is stronger at the bottom than at the surface. This is a feature of the observations that is being investigated separately (H. Seim, personal communication, 2002). The average current for the second winter period is poleward, suggesting that despite the wind direction, baroclinic effects can control the net flow.

5. Discussion

[45] The results show the seasonal heating and cooling of the SAB shelf waters. In conjunction with the net heat flux estimates from *Atkinson et al.* [1983], who examined the net heat flux for the SAB by computing the temperature change in the top 10 m of shelf water, the following (previously observed) cycle is evident. Winter stratification on the inner to mid-shelf is weak at less than 0.5 σ_t. The shelf break is permanently stratified, with the strongest stratification in summer. Surface waters warm significantly between March and April, as the net heat flux becomes positive (into the ocean). The net heat flux peaks in May–June at about 80–90 W m^{-2} [*Atkinson et al.*, 1983], but surface waters continue to warm until July where they remain at about 28°C through September. Stratification is maximum during these months. The net heat flux becomes negative (cooling) by September and the shelf cools rapidly until weak stratification returns in November. A main result, based on the TS diagram distribution (Figure 4) and the cross-shelf transects, is that both temperature and salinity observations are necessary to specify the density distribution on the shelf.

[46] A consequence of the long-term averaging of the TS climatology is that the SAB shelf is essentially permanently stratified on long timescales, even during winter when the

Table 2. Comparison of Mean Cross-Shelf (CS) and Along-Shelf (LS) Depth Averaged Velocity (m s^{-1}) at the Offshore Tower Location Shown in Figure 1[a]

	December–February		May–August	
	CS	LS	CS	LS
CLIM	0.002	0.011	0.001	0.023
R6,1	−0.004	−0.013	0.003	0.033
R6,2	−0.003	0.008	−0.001	0.021

[a]The data have been rotated into cross-shelf and cross-shelf orientation of 31° clockwise from true north. Top row is from the combined (wind- plus density-driven) climatology solutions. The middle (R6,1) and bottom (R6,2) rows are from the R6 tower for summer 2000 and winter 2000–01 (middle) and summer 2001 and winter 2001–02 (bottom). For the along-shelf values, poleward flow is positive and equatorward flow is negative. For the cross-shelf values, offshore flow is positive and onshore flow is negative.

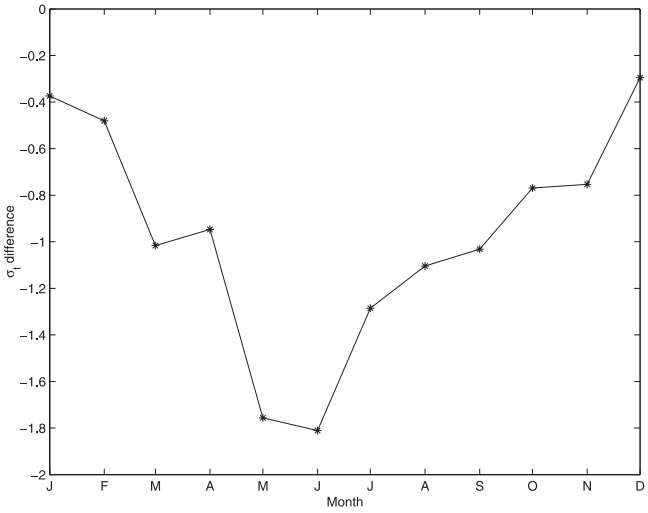

Figure 16. Monthly vertical σ_t difference from the monthly climatology at the tower location R2.

heat loss [*Atkinson et al.*, 1983] and extra-tropical storm activity [*Weisberg and Pietrafesa*, 1983] are maximum. The denser water in the northern SAB subducts under the lighter water in the southern SAB. Figure 16 shows the monthly top-bottom σ_t difference from the monthly TS climatology at the tower R2 location. The winter months (December–February) have small yet still negative top-bottom σ_t differences. This difference increases through June to about -1.8 kg m^{-3}. As the deeper shelf waters continue to warm, this density difference decreases, and continues to decrease through the winter. Recent observations from the R2 tower indicate that monthly average stratification may not be as strong as in the climatology (H. Seim, personal communication, 2002).

[47] The along-shelf poleward flow seen in the density-driven solutions (except in April), which is strongest in January and October, results from the along-shelf elevation gradient that is set up by the off-shelf Gulf Stream and density structure. The elevation decreases in January by about 0.12 m in 6° latitude, which results in an along-shelf slope of about -2×10^{-7}. For July and October, the elevation decrease is about 0.05 m in 6° latitude, or a slope of -1×10^{-7}. These values are in agreement with the range of values from previous studies in the SAB [*Sturges*, 1974; *Atkinson et al.*, 1983; *Lee et al.*, 1984; *Lee and Pietrafesa*, 1987]. The resulting poleward shelf flow decreases in speed toward the coast. The smaller value is the same as that imposed by *Werner et al.* [1993], who found that a slope of -1×10^{-7} drove the shelf-wide flow poleward, with speeds ranging from 0.01 to 0.05 m s^{-1} toward the coast. This is consistent with our July and October results. Unlike previous model studies of the SAB (as noted in section 1), which imposed this gradient as a shelf edge boundary condition, the gradient arises from the derived mass fields and model response, with the elevation on the northern boundary having been specified. The southern boundary elevation is computed to geostrophically balance the transport that arises from the density field.

[48] Figure 17 shows vertical profiles from the separate model solutions averaged over the ADCP observation

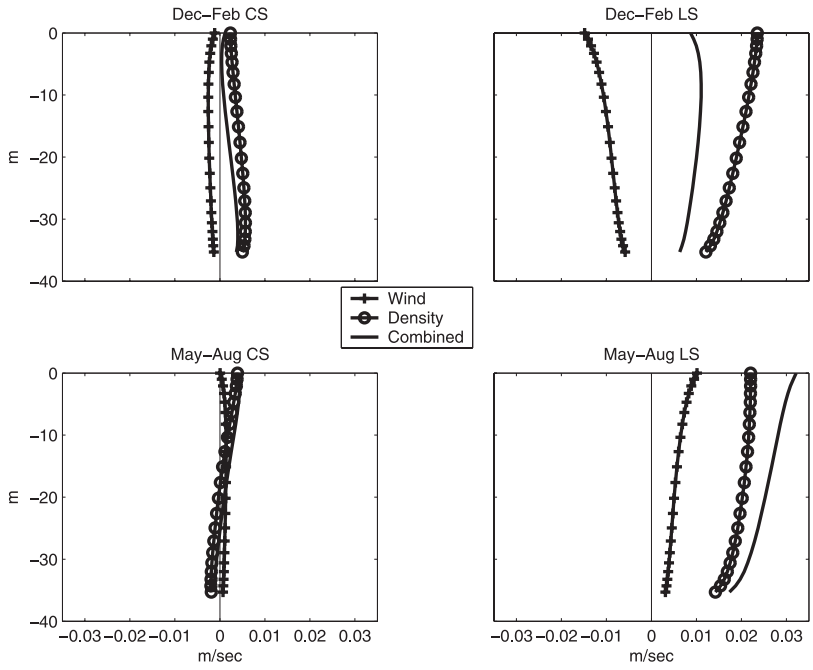

Figure 17. Model climatological velocity profiles at the R6 tower location. Velocities have been rotated into along-shelf (right) and cross-shelf (left) directions. (top) The winter season is over the period December through February and (bottom) summer is defined as May through August. The density-driven flow is shown with circles, the wind-driven flow with plus symbols, and the combined profiles (the same as in Figure 15) with a solid line. For the along-shelf panels, poleward flow is positive and equatorward flow is negative. For the cross-shelf panels, offshore flow is positive and onshore flow is negative. Note that the scale on the abscissa is different than that in Figure 15.

period described previously at the R6 tower location. Over both periods, cross-shelf flows are weak (<0.01 m s^{-1}) in both the wind- and density-driven solutions. Along-shelf flows are stronger (0.01–0.02 m s^{-1}), with the wind-driven flow being poleward during the summer period and equatorward in the winter period. The density-driven flow is poleward during both periods (0.02–0.03 m s^{-1}). The total along-shelf flow at this location is also poleward, with the density-driven flow compensating for the wind-driven component in winter and reinforcing the wind-driven flow in summer.

[49] The derived density fields have significant cross-shelf structure. Despite the presence of cross-shelf density gradients, the contribution of the baroclinic pressure gradient force terms is small. Momentum term estimates (not shown) from the model density-driven solutions indicate that the along-shelf flow seen in July, October, and particularly January is driven primarily by the cross-shelf elevation gradient. The direct contribution from the density field is an order of magnitude smaller than the barotropic pressure gradient component. In the outer shelf, the cross-shelf baroclinic term is of equal importance to the cross-shelf elevation gradient.

[50] The April shelf break density-driven flow (Figure 11b) poleward of the Charleston Bump is probably not representative of the climatological mean, although we expect larger variability in this region. In fact, it is evident (not shown) from the off-shelf objective analysis that the TS observations were biased toward a more off-shelf Gulf Stream position. The resulting along-shelf elevation slope along the 70-m isobath is smaller than that during other months, thus not providing the dominant component to the force balance. The result is that the baroclinic pressure gradient terms are locally more important. In periods when the Gulf Stream is in a more off-shelf position, the local mass field distribution may play a more important role in circulation. On shorter timescales, strong cross-shelf density gradients set up by freshwater river discharge have been shown to be a significant feature in the inner shelf [*Blanton*, 1981; *Kourafalou et al.*, 1996; *Chen et al.*, 1999].

[51] The combined solutions for the monthly SAB response (Figure 11) are in general agreement at the shelf break with the schematic seasonal circulation of *Lee et al.* [1991]; the flow is poleward along the SAB outer shelf, except for the Charleston Bump gyre, which is marginally present in our climatology. Our solutions in the mid-shelf indicate that the flow is composed of approximately equal contributions from wind- and density-driven components. In summer these components reinforce each other; in winter, they are largely equal but opposite. Observations of the mid-shelf flow, however, suggest that the mean mid-shelf flow is generally poleward [*Lee et al.*, 1991]. The inner shelf is dominated by wind-driven flow.

[52] The most significant difference from the *Atkinson et al.* [1983] climatology appears in the October surface salinity. Inner and mid-shelf salinities reach 32 in their results. This is as low as the salinities during the spring river discharge maxima. Our objectively derived October surface and bottom salinity does not show such low salinity. Rather, a relatively smooth transition between months occurs. The source of the low-salinity water is not clear. There is generally not enough river discharge in fall to produce a large volume of low-salinity water in October.

[53] The qualitative character of the diagnostic solutions is relatively insensitive to alternative specifications of bottom stress and vertical mixing. Horizontally constant bottom stress and vertically constant vertical mixing affect the strength of the diagnostic response and shift the position of the "no net flow" regions in the mid-shelf on and offshore. However, the primary sensitivity of the solutions developed here is likely to be stratification effects on the vertical mixing and bottom stress regime. The vertical eddy viscosity is affected by stratification [*Mellor and Yamada*, 1982], which appears to be present in all months on climatological timescales. Generally, the presence of a pycnocline (stratification) tends to decouple upper and lower layers of the water column. *Naimie et al.* [1994] and *Han et al.* [1997] (among others) have shown the sensitivity of model solutions to levels of stratification in tidally driven flows; tidally driven mixing is confined to the lower layers with increased velocities in the upper layers. *Weisberg et al.* [2001] have recently shown the sensitivity of the subtidal wind-driven coastal water levels to the presence of stratification in a numerical experiment of springtime circulation on the west Florida shelf. Considerable improvement in the comparison between modeled and observed water level was demonstrated by inclusion of an appropriate level of stratification with basic springtime characteristics, as opposed to the homogeneous case.

[54] We thus consider our results to be an initial climatology consisting of a diagnosis of the objectively analyzed TS fields with specified mixing. The coupling of the mixing environment to stratification will require prognostic simulations, forced by tides, climatological heat flux and winds, and river discharge (a significant fresh water source in springtime [*Atkinson et al.*, 1983]).

6. Conclusions

[55] We have developed monthly temperature and salinity fields for the South Atlantic Bight shelf based on an objective analysis of available NODC data that show good agreement with the published climatology of *Atkinson et al.* [1983], with the exception of the month of October. The annual heating and cooling of the shelf waters and freshwater river outflow is captured in the monthly TS fields. The associated climatological solutions for the SAB shelf, forced by monthly averaged observed winds and temperature and salinity fields were computed with a steady-state finite element model, made separable due to the linearity of the model. The model solutions confirm previous results in that the wind-driven dynamics are primarily Ekman-like, with strongest upwelling and downwelling along the north Florida shelf. The density-driven flow on the inner shelf is generally weak and dominated by the wind-driven along-shelf flow, except when the wind is weak (April). A more important forcing in the outer shelf is the along-shelf elevation field associated with the off-shelf density field. This provides an cross-shelf elevation gradient that, in conjunction with the baroclinic pressure gradient, generally drives poleward flow.

[56] Historical observational data and observations from the permanent tower installations are not long enough to

represent climatological estimates of the flow. The comparison to recent in situ observations is encouraging, as is the general agreement with previous models of SAB circulation and the GABEX current meter data. However, the observations also show that the fluctuating current is highly variable and due to mechanisms not represented in the climatological wind and TS fields. We expect, however, that the long time series from the tower installations that will eventually cover a large portion of the Georgia coast will be valuable in assessing the character of these and future model solutions.

[57] One immediate use of the monthly TS fields and resulting baroclinic circulation we have derived is for initialization of 2- to 10-day prognostic model simulations for process-oriented studies on the Georgia shelf. Additionally, the TS climatology will be used to initialize a limited-area domain for an operational system designed for real-time hindcasting and forecasting of currents and water levels on the Georgia shelf. Of particular interest is hindcasting the weather-band (subtidal) response on the shelf.

[58] A more complete off-shelf database with XBT data and derived salinity from appropriately defined TS curves will improve the off-shelf climatology. The current level of temporal and spatial resolution of the data is not adequate enough to provide an unbiased estimate of the off-shelf climatology. In some months, there is insufficient data in the off-shelf region to adequately represent the Gulf Stream isopycnic structure and resulting transport. However, the shelf resolution appears adequate.

[59] **Acknowledgments.** We thank J. Bane, T. Shay, and D. Lynch for constructive suggestions, and (particularly B. Blanton) C. Naimie for many years of useful conversations. The comments of two anonymous reviewers significantly improved the clarity and flow of the text. This research was supported by NOPP grants NAG13-00041 and N00014-98-1-0786, and ONR grant N00014-97-1-0500.

References

Atkinson, L. P., T. N. Lee, J. O. Blanton, and W. S. Chandler, Climatology of the southeastern United States continental shelf waters, *J. Geophys. Res.*, *88*, 4705–4718, 1983.

Bane, J. M., Results from the Genesis of Atlantic Lows Experiment physical oceanographic studies: Introduction, *J. Geophys. Res.*, *94*, 10,685, 1989.

Bane, J. M., and W. K. Dewar, Gulf Stream bimodality and variability downstream of the Charleston Bump, *J. Geophys. Res.*, *93*, 6695–6710, 1988.

Blanton, J. O., Ocean currents along a nearshore frontal zone on the continental shelf of the southeastern United States, *J. Phys. Oceanogr.*, *11*, 1627–1637, 1981.

Blanton, J. O., F. B. Schwing, A. H. Weber, L. J. Pietrafesa, and D. W. Hayes, Wind stress climatology in the South Atlantic Bight, in *Oceanography of the Southeastern U. S. Continental Shelf, Coastal Estuarine Stud.*, vol. 2, edited by L. P. Atkinson et al., pp. 10–22, AGU, Washington, D. C., 1985.

Blanton, J. O., T. N. Lee, L. P. Atkinson, J. M. Bane, A. J. Riordan, and S. SethuRaman, Oceanographic studies during GALE, *Eos Trans. AGU*, *68*, 1626–1627, 1636–1637, 1987.

Blumberg, A. F., and G. L. Mellor, Diagnostic and prognostic numerical circulation studies of the South Atlantic Bight, *J. Geophys. Res.*, *88*, 4579–4592, 1983.

Bretherton, F., R. Davis, and C. Fandry, A technique for objective analysis and design of oceanographic experiments applied to MODE-73, *Deep Sea Res.*, *23*, 559–582, 1976.

Bumpus, D., A description of the circulation on the continental shelf of the east coast of the United States, *Prog. Oceanogr.*, *6*, 111–158, 1973.

Chen, C., L. Zheng, and J. O. Blanton, Physical processes controlling the formation, evolution, and perturbation of the low-salinity front in the inner shelf off the southeastern United States: A modeling study, *J. Geophys. Res.*, *104*, 1259–1288, 1999.

Clarke, A., and D. Battisti, The effect of continental shelves on tides, *Deep Sea Res.*, *28*, 665–682, 1981.

Emery, W. J., and J. S. Dewar, Mean temperature-salinity, salinity-depth and temperature-depth curves for the North Atlantic and the North Pacific, *Prog. Oceanogr.*, *11*, 219–305, 1982.

Foreman, M. G. G., R. E. Thompson, and C. L. Smith, Seasonal current simulations for the western continental margin of Vancouver Island, *J. Geophys. Res.*, *105*, 19,665–19,698, 2000.

Greenberg, D. A., F. E. Werner, and D. R. Lynch, A diagnostic finite-element ocean circulation model in spherical-polar coordinates, *J. Atmos. Oceanic Technol.*, *15*, 942–958, 1998.

Han, G., C. G. Hannah, J. W. Loder, and P. C. Smith, Seasonal variation of the three-dimensional mean circulation over the Scotian Shelf, *J. Geophys. Res.*, *102*, 1011–1025, 1997.

Hannah, C. G., J. Shore, J. W. Loder, and C. E. Naimie, Seasonal circulation on the western and central Scotian Shelf, *J. Phys. Oceanogr.*, *31*, 591–615, 2001.

Kantha, L. H., G. L. Mellor, and A. F. Blumberg, A diagnostic calculation of the general circulation in the South Atlantic Bight, *J. Phys. Oceanogr.*, *12*, 805–819, 1982.

Kourafalou, V. H., J. D. Wang, and T. N. Lee, Circulation on the continental shelf of the southeastern United States: III. Modeling the winter wind-driven flow, *J. Phys. Oceanogr.*, *14*, 1022–1031, 1984.

Kourafalou, V. H., L.-Y. Oey, J. D. Wang, and T. N. Lee, The fate of river discharge on the continental shelf: 2. Transport of coastal low-salinity waters under realistic wind and tidal forcing, *J. Geophys. Res.*, *101*, 3415–3434, 1996.

Large, W. G., and S. Pond, Open ocean momentum flux measurements in moderate to strong winds, *J. Phys. Oceanogr.*, *11*, 324–336, 1981.

Lee, T. N., and L. P. Atkinson, Low-frequency current and temperature variability from Gulf Stream frontal eddies and atmospheric forcing along the southeast U. S. outer continental shelf, *J. Geophys. Res.*, *88*, 4541–4567, 1983.

Lee, T. N., and L. J. Pietrafesa, Summer upwelling on the southeastern continental shelf of the U. S. A. during 1981: Circulation, *Prog. Oceanogr.*, *19*, 267–312, 1987.

Lee, T. N., L. P. Atkinson, and R. Legekis, Observations of a Gulf Stream frontal eddy on the Georgia continental shelf, April 1977, *Deep Sea Res.*, *28*, 347–378, 1981.

Lee, T. N., W. J. Ho, V. H. Kourafalou, and J. D. Wang, Circulation on the continental shelf of the southeastern United States: I. Subtidal response to wind and Gulf Stream forcing during winter, *J. Phys. Oceanogr.*, *14*, 1001–1012, 1984.

Lee, T. N., V. H. Kourafalou, J. D. Wang, W. J. Ho, J. O. Blanton, L. P. Atkinson, and L. J. Pietrafesa, Shelf circulation from Cape Canaveral to Cape Fear during winter, in *Oceanography of the Southeastern U. S. Continental Shelf, Coastal Estuarine Stud.*, vol. 2, edited by L. P. Atkinson et al., pp. 33–62, AGU, Washington, D. C., 1985.

Lee, T. N., J. A. Yoder, and L. P. Atkinson, Gulf Stream frontal eddy influence on productivity of the southeast U. S. continental shelf, *J. Geophys. Res.*, *96*, 22,191–22,205, 1991.

Lorenzzetti, J., J. D. Wang, and T. N. Lee, Summer upwelling on the southeastern continental shelf of the U. S. A. during 1981: Circulation modeling, *Prog. Oceanogr.*, *19*, 313–327, 1987.

Lorenzzetti, J., J. D. Wang, and T. N. Lee, Two-layer model of summer circulation on the southeast U. S. continental shelf, *J. Phys. Oceanogr*, *18*, 591–608, 1988.

Lynch, D. R., and F. E. Werner, Three-dimensional hydrodynamics on finite elements: I. Linearized harmonic model, *Int. J. Numer. Methods Fluids*, *7*, 871–909, 1987.

Lynch, D. R., and F. E. Werner, Three-dimensional hydrodynamics on finite elements: II. Non-linear time-stepping model, *Int. J. Numer. Methods Fluids*, *12*, 507–533, 1991.

Lynch, D. R., J. T. C. Ip, C. E. Naimie, and F. E. Werner, Comprehensive coastal circulation model with application to the Gulf of Maine, *Cont. Shelf Res.*, *16*, 875–906, 1996.

Mellor, G., and T. Yamada, Development of a turbulence closure model for geophysical fluid problems, *Rev. Geophys.*, *20*, 851–875, 1982.

Naimie, C. E., and D. R. Lynch, FUNDY5 User's Manual, report, 40 pp., Dartmouth College, Hanover, N. H., 1993.

Naimie, C. E., J. W. Loder, and D. R. Lynch, Seasonal variation of the three-dimensional residual circulation on Georges Bank, *J. Geophys. Res.*, *99*, 15,967–15,989, 1994.

Naimie, C. N., C. A. Blain, and D. R. Lynch, Seasonal mean circulation in the Yellow Sea—A model-generated climatology, *Cont. Shelf Res.*, *21*, 667–695, 2001.

Redfield, A., The influence of the continental shelf on the tides of the Atlantic coast of the United States, *J. Mar. Res.*, *1492*, 432–448, 1958.

Seim, H., Implementation of the South Atlantic Bight Synoptic Offshore Observational Network, *Oceanography*, *13*, 18–23, 2000.

Singer, J. J., L. P. Atkinson, J. O. Blanton, and J. A. Yoder, Cape Romain and the Charleston Bump: Historical and recent hydrographical observations, *J. Geophys. Res.*, *88*, 4685–4698, 1983.

Sturges, W., Sea level slope along continental boundaries, *J. Geophys. Res.*, *79*, 825–830, 1974.

Weber, A. H., and J. O. Blanton, Monthly mean wind fields for the South Atlantic Bight, *J. Phys. Oceanogr.*, *10*, 1256–1263, 1980.

Weisberg, R. H., and L. J. Pietrafesa, Kinematics and correlation of the surface wind field in the South Atlantic Bight, *J. Geophys. Res.*, *88*, 4593–4610, 1983.

Weisberg, R., Z. Li, and F. Muller-Karger, West Florida shelf response to local wind forcing: April 1998, *J. Geophys. Res.*, *106*, 31,239–31,262, 2001.

Werner, F. E., J. O. Blanton, D. R. Lynch, and D. K. Savidge, A numerical study of the continental shelf circulation of the U. S. South Atlantic Bight during the autumn of 1987, *Cont. Shelf Res.*, *13*, 871–997, 1993.

Woodruff, S. D., H. Diaz, J. Elms, and S. Worley, COADS release 2 data and metadata enhancements for improvements of marine surface flux fields, *Phys. Chem. Earth*, *23*, 517–526, 1998.

A. Aretxabaleta, B. O. Blanton, H. E. Seim, and F. E. Werner, Department of Marine Sciences, University of North Carolina at Chapel Hill, 12-7 Venable Hall, CB3300, Chapel Hill, NC 27599-3300, USA. (brian_blanton@unc.edu)

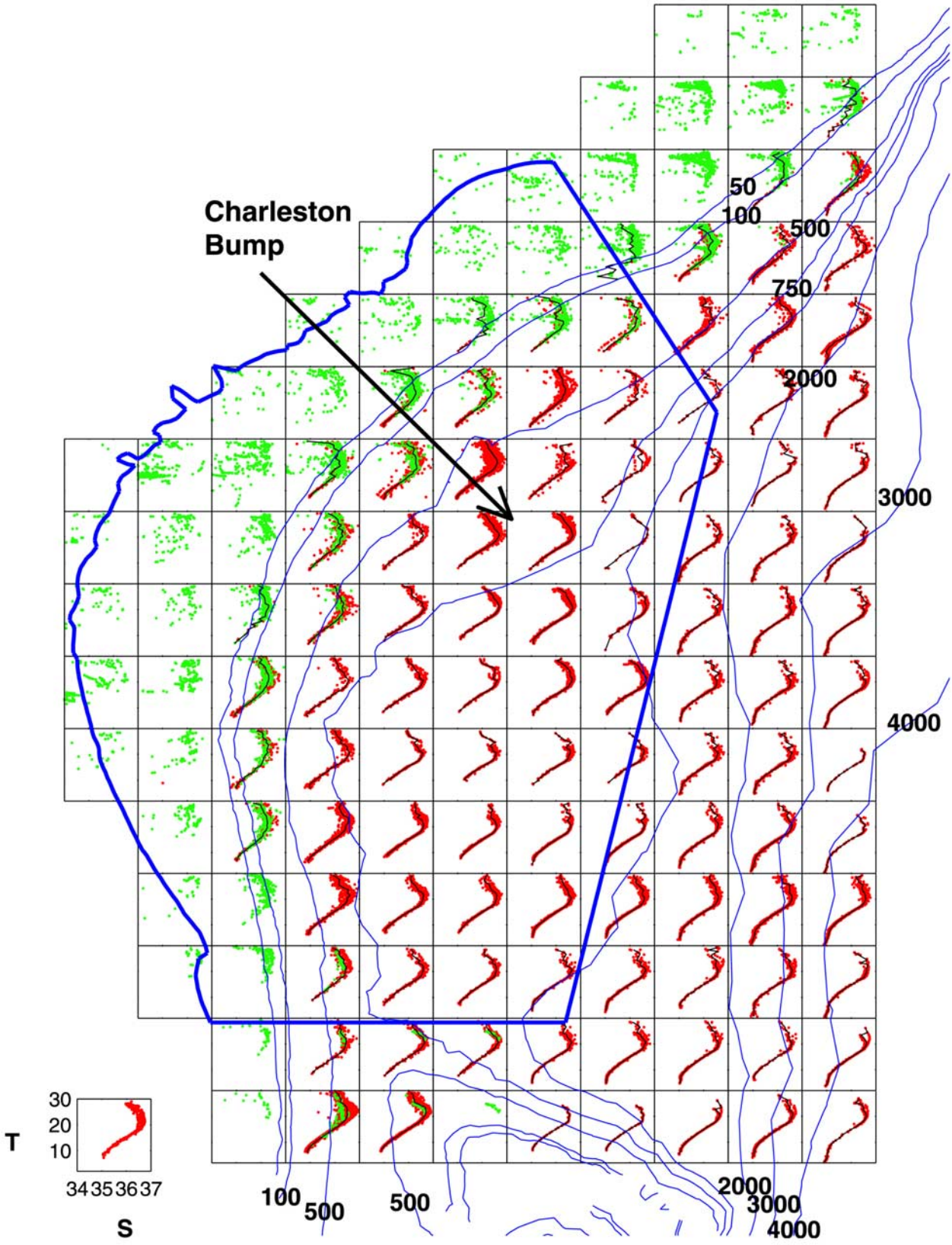

Figure 4. TS diagram distribution. Salinity is on the abscissa; temperature is on the ordinate. The TS curve axis scales for all squares are shown with the separate diagram in the lower-left. Shelf data (<400 m) are in green; deeper water (>400 m) data are in red. For the deep squares, the average TS curve is drawn in black. The 50-, 100-, 500-, 750-, 1000-, 2000-, 3000-, and 4000-m isobaths are shown.